Bone marrow mesenchymal stem cells offer an immune-privileged niche to Cutibacterium acnes in case of implant-associated osteomyelitis

Marie Dubus, Jennifer Varin-Simon, Steve Papa, Julie Chevrier, Fabienne Quilès, Gregory Francius, Sandra Audonnet, Cédric Mauprivez, Sophie C Gangloff, Renaud Siboni, et al.

Acta Biomaterialia (2021), https://doi.org/10.1016/j.actbio.2021.10.026

Bone marrow mesenchymal stem cells offer an immune-privileged niche to *Cutibacterium acnes* in case of implant-associated osteomyelitis

M. Dubus[1,2], J. Varin[1], S. Papa[1], J. Chevrier[1], F. Quilès[3], G. Francius[3], S. Audonnet[4], C. Mauprivez[1,2,5], S. C. Gangloff[1,6], R. Siboni[1,7,8], X. Ohl[1,7,8], F. Reffuveille[1,6], H. Kerdjoudj*[1,2]

1. Université de Reims Champagne Ardenne, EA 4691, Biomatériaux et Inflammation en Site Osseux (BIOS), Reims, France.
2. Université de Reims Champagne Ardenne, UFR d'Odontologie, Reims, France.
3. Université de Lorraine, CNRS, LCPME, F-54000 Nancy, France.
4. Université de Reims Champagne Ardenne, Plateau Technique URCACyt, Reims, France.
5. Centre Hospitalier Universitaire de Reims, Pôle Médecine bucco-dentaire, Hôpital Maison Blanche, France.
6. Université de Reims Champagne Ardenne, UFR de Pharmacie, Reims, France.
7. Université de Reims Champagne Ardenne, UFR de Médecine, Reims, France.
8. Centre Hospitalier Universitaire de Reims, Service d'orthopédie traumatologie, Reims, France.

*Corresponding author at:

Université de Reims Champagne Ardenne, EA 4691, « Biomatériaux et Inflammation en Site Osseux », Pôle Santé, 1 Avenue du Maréchal Juin, 51100 Reims, France.

E-mail address: halima.kerdjoudj@univ-reims.fr (H. KERDJOUDJ)

Abstract:

Considered as some of the most devastating complications, *Cutibacterium acnes* (*C. acnes*)-related osteomyelitis are among the hardest infections to diagnose and treat. Mesenchymal stem cells (MSCs) secrete number of immunomodulatory and antimicrobial soluble factors, making them an attractive treatment for bacterial infection. In this study, we examined MSCs/*C. acnes* interaction and analyzed the subsequent MSCs and bacteria's behaviors. Human bone marrow-derived MSCs were infected by *C. acnes* clinical strain harvested from non-infected bone site. Following 3h of interaction, around 4% of bacteria were found in the intracellular compartment. Infected MSCs increased the secretion of prostaglandin E2 and indolamine 2,3 dioxygenase immunomodulatory mediators. Viable intracellular bacteria analyzed by infrared spectroscopy and atomic force microscopy revealed deep modifications in the wall features. In comparison with unchallenged bacteria, the viable intracellular bacteria showed (i) an increase in biofilm formation on orthopaedical-based materials, (ii) an increase in the invasiveness of osteoblasts and (iii) persistence in macrophage, suggesting the acquisition of virulence factors. Overall, these results showed a direct impact of *C. acnes* on bone marrow-derived MSCs, suggesting that blocking the *C. acnes*/MSCs interactions may represent an important new approach to manage chronic osteomyelitis infections.

Keywords: *Cutibacterium acnes*, implant-associated infection, mesenchymal stem cells, bacteria/ stem cells interactions, bone repair.

1. Introduction

Cutibacterium acnes (*C. acnes*) is a slow growing, lipophilic Gram-positive bacterium that is commonly found in high rates in deep tissue with a great number of sebaceous follicles (*i.e.* skin flora on the chest and back) but also in more than 50% of implant-associated osteomyelitis, particularly those involving shoulder prosthesis infection.[1-3] *C. acnes* related osteomyelitis is one of the most difficult infections to diagnose and care, because of the lack of local inflammatory signs and fistula. Considered as some of the most devastating complications, they require multifaceted and long-term treatments including debridement, administration of intravenous antibiotics, and surgical revision of the implanted device. A broad-spectrum antibiotic treatment is often inefficient due to locally damaged vasculature and the formation of biofilms. Furthermore, surgical debridement compromises the regenerative capacity of the bone leaving behind a large “dead space”. Therefore, implementation of effective strategies to improve the management of *C. acnes*-related implant-associated osteomyelitis has become a therapeutic challenge.

Exciting recent advances in the understanding of *C. acnes*-related osteomyelitis can be found in studies focused on microbiological methodology. Because of its anaerobic metabolism, *C. acnes* cannot be reliably detected by culture in aerobic standard conditions and need a long time to grow (5 to 7 days).[4] Up-to-date, the ongoing controversies exist concerning the origin of *C. acnes* infections. Few reports construct a reasonable hypothesis about a probable leakage of bacteria from the superficial skin into the surgical wound after incision despite a strict aseptic procedure (*i.e.* skin preparation using alcoholic chlorhexidine or alcoholic polyvidone, antibiotic prophylaxis).[5,6] More recently, Hudek and collaborators reported the presence of

commensal *C. acnes* in deep intra-articular tissues. Indeed, *C. acnes* was detected in the intracellular compartment of macrophages and stromal cells in 62.5% of the tested patients who did not undergo skin penetration (*i.e.* by surgery or injection).[7,8]

Among bone stromal cells, mesenchymal stem cells (MSCs) are predominantly found in bone marrow and periosteum and are the source of osteogenic lines of cells capable of forming bone matter. It is now widely assumed that MSCs secrete a number of soluble factors, that regulate inflammation and immune responses or kill bacteria, which make them an attractive treatment against bacterial infection.[9-12] In opposition to the beneficial effect of intravenously administered MSCs for sepsis treatments, recent researches reported negative effects of MSCs on the treatment of *Staphylococcus aureus* (*S. aureus*)-related osteomyelitis.[13,14] The presence of both *S. aureus* and *C. acnes* strains was recently detected in bone marrow-derived MSCs cytoplasm, following *in vitro* challenging.[15-17] These intracellular bacteria are thought to be responsible for chronic and recurrent infections. Furthermore, MSCs challenged with *C. acnes* adopted an immune suppressive profile.[15] Thus, the excessive immune suppression can lead to an undesirable effect; hampering the host's ability to fight the infection and, instead, encouraging the spread of the bacterial infection.

C. acnes colonization of MSC's cytoplasm has been recently demonstrated without inducing a cytotoxic effect on MSCs.[15,17,18] However, to date there has been no published experimental or clinical studies highlighting that the commensal *C. acnes* can develop a "pathogenic" behavior following their release in the extracellular environment. Aiming to increase knowledge on *C. acnes*-related osteomyelitis and to elucidate the underlying immunological and microbiological mechanisms, this study used human bone marrow-derived MSCs and a bone commensal *C. acnes* clinical strain. To assess the effect of MSCs/*C. acnes* interaction in the establishment of

chronic implant infections, the results were compared to *C. acnes* clinical strain isolated from an infective implant. The findings reported here indicate that commensal *C. acnes* were able to activate the immunomodulatory profile of MSCs. Unlike *C. acnes* isolated from the infective implant, the bone isolated strain modified its nano-scaled wall characteristics reaching the features of infected implant isolated strain. These bacteria increased (i) the biofilm formation on orthopaedical-based materials, (ii) the invasive capability of bone forming cells and (iii) the resistance to macrophage clearance through an increase in catalase production. These findings suggest that blocking the *C. acnes*/MSCs interactions may represent an important new approach to manage chronic osteomyelitis infection.

2. Experimental

***C. acnes* culture:** Clinical *C. acnes* isolated at the laboratory of Reims University Hospital Center (CHU Reims) were used in this study. The first one, named Cb, was isolated frombone specimen of a patient for which no clinical bone infection was established. The second one, named Ci, was isolated from a patient's implant with a confirmed orthopaedic implant-associated infection. Bacteria were isolated on Columbia agar with 5% of sheep blood under anaerobic conditions using Genbox system (Biomerieux, France). For all experiments, *C. acnes* were cultured for 5 days in Brain Heart Infusion (BHI) broth under anaerobic conditions. Bacteria were washed and resuspended in sterile Dubelcco's phosphate buffered saline (DPBS, Gibco, France) for the co-culture experiments.

Eukaryote cells culture: Human specimen (bone marrow and mandibular bone) and THP-1 cell lines were used in this study. Human specimen (bone marrow and mandibular bone) harvestings were approved ethically and methodologically by our local Research Institution and were conducted with informed patients (written consent,

non-opposition) in accordance with the usual ethical legal regulations (Article R 1243-57). All procedures were done in accordance with our authorization and registration number DC-2014-2262 given by the National ‘‘Cellule de Bioéthique’’. Human bone marrow samples, from at least 6 healthy donors, were collected by aspiration from femoral necks of patients (aged between 40 and 70 years old) undergoing total hip replacement. Aspirated bone marrow was diluted in PBS (*v/v*) and centrifuged at 300 *g* for 10 min. Primary cultures (P0) were initiated by plating isolated mononuclear cells at 5×10^5 cells/cm^2 in α-MEM (Lonza, France) supplemented with 10% decomplemented fetal bovine serum (FBS), 1% Penicillin/Streptomycin/Amphotericin B (PSA) and 1% Glutamax® (*v/v*, Gibco, France) and maintained in a humidified atmosphere of 5% CO_2 at 37 °C. Mesenchymal stem cells (MSCs) were washed twice a week with DPBS to remove non-adherent dead cells. Viable MSCs were at all times cultured at 37 °C and 5% CO_2 in a humidified atmosphere with a medium change every two days. MSCs were expanded upon the second passage and characterized by flow cytometry LSRFortessa BD Biosciences, France) through the expression of CD73, CD90, CD44, CD105, CD34, CD14, and HLA-DR and used in our experimental procedure at the third passage. Human mandibular bone specimens without any clinical or radiographic evidence of pathology were obtained from young patients (aged between 13 and 33 years old) undergoing wisdom teeth extraction oral surgery. After extensive (four to five times) washing steps, bone specimens were scraped to remove attached soft tissue and periosteum, broken into small pieces and predigested for 1 h with trypsin-EDTA (0.5%, *v/v,* Gibco, France) / B collagenase (1 mg/mL, Sigma France) in a serum-free Dulbecco's Modified Eagle medium (DMEM, Gibco, France). Fragments were then placed into 25 cm^2 tissue culture flask and maintained in a humidified atmosphere of 5% CO_2 at 37 °C, thus allowing osteoblasts migration and

proliferation in the presence of DMEM supplemented with 20% FBS and 1% Penicillin/Streptomycin (*v/v*, Gibco, France). Osteoblasts were then amplified at a density of 10^4 cell/cm^2 in 10% FBS supplemented DMEM with a medium change twice/week and used at the third passage in our experimental study design. THP-1 cell line, cultured in RPMI supplemented with 10% FBS and 1% Penicillin/Streptomycin, were seeded at 2.6×10^5 cells/cm^2 in 24 well plate and differentiated into macrophage by adding 50 mM phorbol 12-myristate 13-acetate (PMA, Sigma, France) for 48 h then used in our experimental study design.

***C. acnes*/MSCs interactions:** MSCs were seeded in 24-well plates at 10^3 cells/cm^2. After 72 h of culture, cells were washed with DPBS and cultured, overnight, with 1 mL per well of PSA-free culture medium. The next day, cells were washed twice with DPBS and 1 mL of PSA free culture medium and exposed to live bacteria to obtain a multiplicity of infection (MOI) 30:1. After 3 h of interaction, gentamicin-based antibiotic protection assay was performed. Cells were washed extensively with DPBS and incubated for 1 h with culture medium supplemented by 100 µg/mL of gentamicin (Fisher scientific, France). Cells were then washed extensively with DPBS maintained in culture for 48 h or lysed with 0.1% Triton X-100 (Sigma, France). The intracellular lysates were seeded on Columbia blood agar plates using Easyspiral (Intersciences, France) and incubated at 37° C for 5 days in anaerobic conditions. The rate of viable intracellular *C. acnes* was determined after bacterial colony count. After 48h of culture, supernatant of infected MSCs were seeded on Columbia blood agar plates and cultured as previously described (bacteria used for THP-1 and osteoblast infection) or preserved at -20 °C (for ELISA analysis).

Cytochalasin D assay and *C. acnes* infection: MSCs were seeded in 24-well plates at 10^3 cells/cm^2. After 72 h of culture, MSCs were washed with DPBS and cultured,

overnight, in PSA-free culture medium supplemented with 0.1µg/mL cytochalasin D (Sigma, France). Cytochalasin D-treated cells were infected with Cb and Ci and the intracellular rate of alive bacteria was determined as previously described.

***C. acnes*/Osteoblast interactions:** Osteoblasts were seeded in 24-well plates at 10^3 cells/cm^2 and cultured for 72 h. Following culture overnight in 1 mL per well of PSA-free culture medium, osteoblasts were exposed to live bacteria isolated from MSCs supernatant with MOI of 100:1. After 3 h of interaction, gentamicin-based antibiotic protection assay was performed. The intracellular rate of alive bacteria was analyzed as previously described.

Macrophage phagocytosis and persistence: Differentiated THP-1 were washed with DPBS and cultured, overnight, with 1 mL per well of PSA-free culture medium. The next day, cells were washed twice with DPBS and exposed to live bacteria isolated from MSCs supernatant with MOI of 1:1. After 2 h of interaction, gentamicin-based antibiotic protection assay was performed. One part of the cells was used for the intracellular quantification of alive bacteria and the other was maintained in culture for 24h before the quantification of alive bacteria. The intracellular rate of alive bacteria was analyzed as previously described.

Confocal laser scanning microscopy: *C. acnes* labelled by 4',6-diaminido-2-phenylindole (DAPI, 1/1000 dilution in DPBS) were used for MSCs infection. After 3 h of interaction with MSCs, cells were rinsed with DPBS, fixed with 4% paraformaldehyde (Sigma-Aldrich) at 37°C for 15 min and permeabilized with 0.5% Triton X-100 for 10 min. MSCs were then incubated for 30 min at room temperature with Alexa® Fluor-488 conjugated-Phalloidin® (1/100 dilution in DPBS, Invitrogen). After washes, cells were incubated for 5 min with DAPI (1/3000 dilution in water, Invitrogen). Stained cells were mounted and imaged by confocal microscopy (CLSM

710, NLO, Zeiss, Germany). Image analysis was performed using ImageJ.

Scanning electron microscopy (SEM): *C. acnes*-infected MSCs were washed twice with DPBS and fixed in 2.5% glutaraldehyde at room temperature, for 1 h. After two sterilized water rinses, samples were dehydrated in graded ethanol solutions (50, 70, 90 and 100%) for 10 min and desiccated in a drop of hexamethyldisilazane (HMDS). After air-drying at room temperature, samples were sputtered with a thin gold-palladium film using a JEOL ion sputter JFC 1100 instrument. Samples were observed using a Schottky Field Emission SEM (JEOL JSM-7900F).

Transmission electron microscopy (TEM): *C. acnes*-infected MSCs were rinsed with cacodylate buffer solution (125 mM), fixed in 2% paraformaldehyde and 2.5% glutaraldehyde in 50 mM cacodylate buffer at pH 7.4 for 2 h at room temperature and finally post-fixed in 1% osmium tetroxide in 125 mM cacodylate buffer for 30 min. Samples were dehydrated for 15 min in solutions with gradually increasing concentration of ethanol. Samples were then embedded in epoxy resin (48.2% epon 812, 34% anhydride nadic methyl, 16.4% anhydride [2-dodecenyl] succinic, and 1.5% 2,4,6-tris dimethylaminoethyl] phenol) for 48 h at 60 °C. After resin polymerization, a thermic shock in liquid nitrogen was first performed to remove the substrate. To obtain transversal sections of embedded samples, the cutting surface was reoriented by preparing a small block using a circular saw (Bronwill Scientific) and sticking them on new ones. Ultra-thin cross sections (100 nm in thickness) were performed using an automatic ultra-microtome (Ultracut-E Ultramicrotome, Reichert Jung). The specimen was observed with a TEM (JEOL) operating with an accelerating voltage of 70 kV. Images were captured on SO163 Kodak films.

Intracellular accumulation of reactive oxygen species: Following 2 h of *C. acnes*/differentiated THP-1 interaction and gentamicin treatment, cells were detached

by EDTA-trypsin (Gibco) and labelled using Muse oxidative stress kit (Luminex), following the manufacture's recommendation. Samples were analyzed by flow cytometry (LSRFortessa BD Biosciences).

Enzyme-linked immunosorbent assay (ELISA): After *C. acnes* infection, MSCs were maintained in culture for 48 h and supernatants were collected, filtered and stored at -20 °C. Secreted levels of IDO and PGE-2 were assessed in supernatants using respectively Human IDO DuoSet (R&D systems) and PGE2 Express ELISA Kit (Cayman chem), according to the manufacturer's instructions. Optical densities were measured using a microplate reader (FLUOstar Omega microplate reader, BMG Labtech); the amount of cytokines released was calculated from the corresponding standard curves.

Biofilm assays: One colony of bacteria (isolated on agar plate) was added in 1 mL of BHI in 24 well plate containing titanium (TA6V), steel (316L SS), polyetheretherketone (PEEK) and COL-I coating glass (100 µg/mL). After 5 days, plates were then gently washed and (i) incubated with 1 mL of 0.2% crystal violet for 20 min, washed and absorbed crystal was dissolved in ethanol (95%) before absorbance measurement (FLUOstar Omega microplate reader, BMG Labtech at 595 nm); (ii) stained using the Live/Dead Baclight Bacterial Viability kit (Molecular Probes). After 30 min of incubation in the dark at room temperature, biofilms were washed twice in PBS and imaged using confocal laser scanning microscopy (CLSM 710, NLO, Zeiss, Germany). Image analysis was performed using ImageJ.

Infrared spectroscopy (IR): IR spectra in attenuated total reflection (ATR) mode were recorded on a Bruker Tensor 27 spectrometer equipped with a KBr beam splitter and a DTGS detector. The Bruker OPUS 7.5 software drove the spectra recording and the data processing. The resolution of the single beam spectra was 4 cm^{-1}. Two hundred

scans were collected per spectrum corresponding to a 2 min accumulation time. All interferograms were Fourier processed using the Mertz phase correction and a Blackman-Harris three-term apodization function. A nine-reflection diamond ATR accessory (DurasamplIR™, SensIR Technologies, incidence angle: 45°) was used for acquiring spectra. No ATR correction was performed. IR spectra are shown with an absorbance scale corresponding to log10 (Rreference/Rsample), where R is the internal reflectance of the device. One drop of the bacterial suspension in PBS was laid on the ATR crystal. The spectral background was removed by recording the spectrum of sterile DPBS. Water vapor subtraction was performed when necessary. All spectra were baseline corrected at 1800 and 900 cm^{-1}. Measurements were performed at 22 ± 1 °C in an air-conditioned room.

Atomic force microscopy (AFM): *C. acnes* suspensions were deposited and sorbed onto glass slides previously coated with polyethyleneimine (PEI at 2% in water) for 30 min. Samples were rinsed with PBS before being placed into AFM-closed fluid cell for nano-indention measurements. Nanomechanical properties of the deposited bacteria were performed using a MFP3D-BIO instrument (Asylum Research Technology, Oxford Instruments Company, Wiesbaden, Germany) by recording at least 3 Force Mapping Images (FMI) at different locations of the sample. Each FMI consisted of a grid of 40 × 40 force curves measured with adopting an approach rate of 1 µm/s of the tip toward the sample. The Young modulus *E* was evaluated by analyzing the force-indentation curves within the framework of the Sneddon model.[19,20] In this model, the Young modulus is related to the applied force according to the equation given below:

$$F = \frac{2E \tan\theta}{\pi(1-\nu)} R^{1/2} \delta^2 f_{BECC}$$

where δ is the indentation depth, ν the Poisson coefficient, θ the semi-top angle of the

conical tip and f_{BECC} is the bottom effect cone correction function[20] that consider the stiffness of the silicon wafer substrate that supports the vesicles. All FMI were analyzed using an automatic Matlab algorithm detailed elsewhere[21] and average or median Young's moduli values given in this work were derived from at least 1,000 force curves collected over all FMI. For imaging, the same samples were slightly dehydrated. Imaging measurements were performed using a Bioscope Resolve (Bruker Nano Surface, Bruker France SAS, Palaiseau, France). Bacterial morphology was addressed by AFM operating in peakforce tapping™ mode using silicon nitride cantilevers purchased from Bruker (PeakForce HIRS-SSB, Bruker France SAS, Palaiseau, France) with spring constant of about 0.12 nN/nm. All images were recorded with a resolution of 512 × 512 pixels for a scan rate of 0.5 Hz and a maximal applied force of about 0.5 nN.

Catalase activity: *C. acnes* catalase activity was evaluated using catalase activity colorimetric/fluorometric assay kit (MBL international) following the manufacture's recommendation. Briefly, after five days of *C. acnes* culture the absorbance at 600 nm was adjusted at 1 in order to obtain 10^9 bacteria for each condition. After DPBS washes, bacteria were lysed in 200 µL of cold assay buffer supplemented by 10 mg/mL lysozyme and 40 µL of supernatant was deposited in 96-wells plate with 38 µL of assay buffer and incubated for 5 min, at 25 °C then 12 µL of H_2O_2 was added and the plate was incubated for 30 min at 25 °C. 10 µL of stop solution was then added as well as mix solution containing cold assay buffer, Oxired and HRP. After 10 min, at 25 °C, absorbance was measured at 595 nm. A high control, containing 10 µL of stop solution before the first incubation, was carried out for each sample.

Statistical analyses: All statistical analyses were performed using GraphPad Prism 6 software. Experiments of MSCs/bacteria interaction were performed in duplicate with

human bone marrow samples from 6 independent healthy donors. Experiments of osteoblasts/bacteria interaction were performed in duplicate with osteoblasts from 3 independent healthy donors. AFM and IR spectroscopy were performed with intracellular bacteria from three independent MSC's donors. Histogram plots represent mean ± SEM, statistical analyses were performed using Mann & Whitney test. For each test, a value of $p < 0.05$ was accepted as statistically significant *p*.

3. Results and discussion

C. acnes has been associated with multiple post-operative complications involving the biofilm formation, a persistent post-operative pain, and chronic inflammation. Recently, *C. acnes* were identified as commensal bacteria of the osteoarticular site.[7] Herein, the pathogenicity of *C. acnes* in the context of bone repair was investigated. For that purpose, bacteria were harvested from non-infected bone site (hereafter named Cb). The behavior of Cb strain was compared to *C. acnes* isolated from infected orthopaedical implant (hereafter named Ci). To avoid the disparities in protein expression,[22] both selected Cb and Ci exhibit the same multilocus sequence typing and phylotype (*i.e.* CC1, IA1, respectively). Although the virulence factors of *C. acnes* are harder to pinpoint, biofilm formation has emerged as a potential key feature associated with virulence.[2,23-25] Therefore, by analyzing the bacterial behavior, we noticed that both clinical *C. acnes* strains were able to produce biofilm structures on orthopaedical materials [i.e. titanium alloy (TA6V), 316L stainless steel (316L SS) and polyetheretherketone (PEEK)] **(Figure SI-1)**. Crystal violet assay indicated that Ci strain formed a dense biofilm on TA6V compared to Cb strain **(Figure SI-1A)**. Confocal laser scanning microscopy (CLSM) revealed that both strains formed a thicker biofilm on TA6V, however, the analysis of the total covered area indicated a significant

increase in total covering area for Ci on 316L SS and PEEK materials compared to Cb **(Figure SI-1B and C)**. Taken together, these results highlighted the higher virulence-*like* profile of Ci *versus* Cb.

3.1. MSCs/*C. acnes* interaction: Bone marrow, the main source of regenerative mesenchymal stem cells (MSCs), is encased within bone. Following infection, MSCs are thought to provide a protective niche for bacteria from the immune system.[15,17,18,26,27] Herein, we investigated whether human bone marrow-derived MSCs could provide a protective niche for the Cb strain. To this end, primary cultured MSCs were challenged for 3 h with Cb according to the acute infective model[28] and the infective capabilities of Cb were compared to the Ci strain. The gentamicin-based antibiotic protection assay and cell lysis revealed that the rate of the viable Cb and Ci within MSC's cytoplasm was about 4% and 6%, respectively **(Figure 1A)**. Cb showed however a lower invasiveness than Ci (~ 1.4-fold lower, $p = 0.01$), suggesting a higher pathogenicity of Ci since they could contribute for spreading the infection. For better comprehension, we designated viable intracellular Cb as Cb-MSCs and viable intracellular Ci as Ci-MSCs. The ultrastructural analysis of infected MSCs confirmed the presence of electron-dense structures in MSC's cytoplasm. Surprisingly, bacteria were not located in vacuoles but were free in the cytoplasm **(Figure 1B)**. Scanning electron microscopy observations corroborated by CLSM pictures of stained cytoskeleton that showed the absence of cell damage following infection, since we noticed the presence of actin bundles and an elongated morphology **(Figure 1C and 1D)**. Noticed that DAPI labelled Cb were mainly localized between F-actin fibers, confirming their intracellular localization.

The plasma membrane of eukaryotic cells is a dynamic structure that coordinates the

entry of macromolecules and cells.[29] *C. acnes,* a lipophilic strain, possesses specific metabolic features[30] that could participate to the passage through the eukaryote lipid bilayer membrane. This raises questions about the internalization of bacteria by MSCs. To examine the potential role of MSCs in *C. acnes* invasion, MSCs were treated with cytochalasin-D (cyto-D) for 24 h prior bacteria challenging. Cyto-D, a class of fungal metabolites, affects a wide variety of motile functions of eukaryotic cells, by inducing depolymerization of actin filaments **(Figure SI-2)**. Gentamicin-based antibiotic protection assay and cell lysis revealed that cyto-D treatment did not block the entry of *C. acnes* in MSCs. The rate of the viable bacteria was however < 2% for both Cb and Ci strains. Compared to untreated MSCs, ~ 25% of both strains were detected in cyto-D-treated MSCs **(Figure 1E)**. These results suggest that *C. acnes* possess specific metabolism allowing eukaryote cytoplasm invasion. These results need to be comforted by further investigations by using other non-phagocytic cells such as osteoblasts and fibroblasts but also through a deep analysis of lipophilic metabolism of *C. acnes.*

3.2. Impact on the immunomodulatory behavior of MSCs: Activated by the injury, MSCs respond by secreting a spectrum of bioactive molecules, making them extremely useful in the treatment of infective diseases (sepsis, lung…).[11,12] Therefore, to be curative, MSCs must not only release antimicrobial peptides to kill bacteria but also must release immunomodulatory molecules such as prostaglandin E2 (PGE-2) and indolamine 2,3 dioxygenase (IDO) to promote the clearance of bacteria by the immune cells.[12] To assess the immunomodulatory profile of infected MSCs, cells were maintained in culture for 48 h and the supernatant was analyzed by ELISA. The released IDO and PGE-2 by Cb and Ci-infected MSCs were compared to protein levels

secreted by non-infected cells. Interestingly, while Cb increased significantly the PGE-2 and IDO production (> 2-fold increase *versus* the MSCs basal production, $p<0.01$), Ci showed an effect on PGE-2 production but not on IDO **(Figure 2)**. It is well known that these mediators are involved in the regulation of the macrophage plasticity. Indeed, based on the specific microenvironment of MSCs, macrophages may be polarized into classically activated antimicrobial and proinflammatory M1 macrophages or alternatively activated M2 macrophages, that are able to alleviate inflammation and to boost the tissue repair.[11,12] These results suggest that Cb-infected MSCs, through their trophic activities, might establish a regenerative microenvironment to support the regeneration of the injured tissue instead of fighting the bacteria infection. The privileged M2 macrophages could in part explain the "low grade" resulting infection and the lack of local inflammatory signs in clinic. Therefore, we thought that a local administration of MSCs during prosthesis surgery could impair prosthesis osteointegration and increase chronic implant-associated osteomyelitis.

3.3. Impact on the physicochemical features of the *C. acnes* wall: An increase in the bacterial pathogenicity could be a result in bacteria wall modification.[31-33] The physicochemical characterization of the *C. acnes* wall is thus crucial to understand their pathogenicity. Infrared spectroscopy (IR) is a method used to identify molecular compounds of a wide range of sample types including living microorganisms.[34,35] Herein, the spectral features Cb-MSCs and Ci-MSCs as well as Cb and Ci gathered common biochemical components of bacterial cells [proteins (*i.e.* amide I and II bands from proteins located at 1644 and 1550 cm^{-1}, respectively), nucleic acids, phospholipids and teichoic acids (*i.e.* 1250−1190 cm^{-1} and 1180 − 950 cm^{-1}), and polysaccharides (mainly located at 1180 − 950 cm^{-1})]. The IR band assignments were

made according to the literature[36,37] and are indicated in the **Figure 3**. A significant reduction in spectra intensity for polysaccharides with respect to amide II band was observed for Cb-MSCs in comparison with Cb. Indeed, ratios amide II / polysaccharides of integrated intensities were 1.02 for Cb-MSC versus and 0.76 for Cb, suggesting a change in the carbohydrate amount and composition following MSCs invasion. From the reduction in the intensities of bands at (i) 1151 and 1020 cm^{-1} and at (ii) 1079 and 1050 cm^{-1}, it might be suggested that mainly amounts of α- and β-glugans were reduced in Cb-MSCs, respectively.[38] Ratios amide II / polysaccharide of integrated intensities are 0.92 for Ci-MSCs and 0.83 for Ci. In accordance with the values of these ratios, Ci-MSCs exhibited a similar fingerprint to Ci, suggesting that Ci were weakly impacted following MSC's cytoplasm invasion. Glucans are involved in various physiological processes including anti-tumor, antioxidant activities as well as enhancing macrophage activity.[39-41] Thus, herein a reduction in the glucan content in Cb-MSCs might have impaired the macrophage activity following phagocytosis. MSCs exert a direct antimicrobial effect through the secretion of antimicrobial peptides.[42,43] In this study, the IR spectra, did not reveal the presence of stress markers as polyhydroxyalkanoate or glycogen in either Cb-MSCs and Ci-MSCs,[44,45] suggesting that *C. acnes* are not sensitive to the antimicrobial action of MSCs.

3.4. Impact on the nano-scaled features of *C. acnes* wall: The peptidoglycan layers of Gram-positive bacteria are densely functionalized with macromolecules such as exopolysaccharides and teichoic acids.[31] These macromolecules play crucial roles in cell shape and function such as interactions with immune cells or various surfaces.[33] Atomic Force Microscopy (AFM) has the ability to observe single bacteria at nanometer resolution resulting in an opportunity to study in depth the features of the bacterial wall.

A closer look on the bacterial morphology on the nanoscale, carried out by AFM, revealed that Cb were more elongated and softer (2.9 ± 2.3 µm; 247.7 ± 93 kPa) than Ci (1.6 ± 1.1 µm; 797 ± 116 kPa), but their diameter remained in the range of 0.6 up to 1.0 µm (**Figure 4A**). Although the results did not reveal major changes in bacteria morphology following MSCs infection, bacterial wall features were deeply affected by the MSCs invasion. Indeed, a close inspection of bacterial surfaces revealed that Cb-MSCs exhibited shorter parietal macromolecules associated with a lower bacterial adhesion in terms of magnitude in comparison with Cb (~1.36-fold lower, $p<0.0001$). Interestingly, an opposite behavior was observed for Ci-MSCs with an increase in the parietal macromolecules length and bacterial adhesion *versus* Ci (**Figure 4B** and **4C**). From a biomechanical point of view, Cb-MSCs showed a significant increase in elasticity in comparison with Cb (~ 2-fold higher, $p<0.0001$). Such stiffening could result from the removal of macromolecule layer as reported in literature.[46-49] Inversely, Ci-MSCs showed an increase in elasticity (~2.5-fold higher, $p<0.0001$), while force measurements revealed the presence of numerous and long macromolecules in comparison with Ci (**Figure 4D**). These AFM results are in line with the above mentioned biochemical infrared fingerprint that revealed significant modification in Cb-MSCs an alteration of the carbohydrate composition following MSCs invasion, but surprisingly, were not in agreement with Ci-MSCs biochemical fingerprint. As Ci-MSCs exhibited a similar fingerprint to Ci, one can hypothesize that the long macromolecules detected in AFM could be originate from cytoplasmic residues that were not removed in the AFM sample. Taken together, these results suggest that MSCs internalization affects mainly the commensal bacterial wall features that seem close to those measured for Ci infective bacteria.

Impact on the biofilm formation: It is well established that bacterial biofilm plays an important role in the pathogenesis of many human infections. One of the striking properties of bacteria growing in a biofilm is their increased resistance to antimicrobial agents.[50,51] Herein, we investigated if viable intracellular bacteria increased the biofilm formation on orthopaedic implant materials. Type I collagen (COL-I), the main organic part of the bone extracellular matrix, was also studied. Biofilm formation on TA6V, 316L SS, PEEK and COL-I was determined by crystal violet assay and the results were normalized to the non-exposed bacteria to MSCs (**Figure 5**). Raw data are provided in supplementary data (**Figure SI-3)**. The results revealed that the bacteria behavior seems strongly linked to the material. In comparison with Cb, Cb-MSCs significantly increased the formation of biofilm on TA6V and PEEK (at least 2-fold increase) but reduced the biofilm formation on 316L SS and COL-I. Ci-MSCs showed a significant increase in biofilm formation on PEEK and COL-I *versus* Ci, while no difference in biofilm formation was noticed on TA6V. Ci-MSCs showed also a significant decrease in biofilm formation on 316L SS (**Figure 5A**). CLSM visualization of live/dead stained bacteria showed the presence of numerous and thick aggregates on TA6V. On 316L SS, PEEK and COL-I biofilms of both strains seemed quite similar with few live sporadic clusters of bacteria (**Figure 5B**). To sum-up, Cb-MSCs and Ci-MSCs adopted different biofilm behaviors on non-living bone materials. Titanium alloy remains the preferential surface for *C. acnes,* even more so for Cb-MSCs (that reached Ci-formed biofilm (p=0.12)), supporting the hypothesis of the potential transition of Cb from commensal to an opportunistic pathogen after MSCs infection.

Impact on bone cells: As mentioned above, *C. acnes* have been detected in osteoarticular stromal cells.[7] The above results showed deep changes in bacterial wall

features of Cb-MSCs reaching those of pathogenic Ci. Herein, we investigated whether these changes affected the *C. acnes* bone environment cell interactions, in other words, whether Cb-MSCs are able to invade neighbor bone environment cells such as osteoblasts and resident macrophages. For that, infected MSCs were maintained in culture for 48 h and bacteria released in the supernatant were used for primary human osteoblasts challenging. Cb and Ci strains non-exposed to MSCs were used as control. Gentamicin-based antibiotic protection assay and cell lysis showed that Ci and Cb were able to invade osteoblast cytoplasm; the rate of the viable bacteria was ~ 1.5 % for both strains, lower than above MSCs-related results (**Figure SI-4A**) but is consistent with the results obtained for MG63 and SAOS-2 osteoblastic cell lines.[18] Compared to the bacteria control, the osteoblast intracellular rate of Cb-MSCs increased significantly (2-fold, *versus* Cb p=0.02), while no difference was noticed for Ci-MSCs (**Figure 6A**). These results suggest that commensal Cb following infection of MSCs acquires features that increase osteoblast infection.

Tissue-resident macrophages are a population of immune cells that fulfill tissue-specific and niche-specific functions (*i.e.* clearance of cellular debris, response to infection, resolution of inflammation). In this study, PMA differentiated THP-1 were challenged with Cb-MSCs and Ci-MSCs harvested in MSC's supernatant following 48 h of culture. Cb and Ci were used as control. The quantification of the extracellular bacteria after 120 min of infection showed that ≈ 50% of bacteria were phagocyted whatever the studied strain (**Figure SI-4-B-E**). After 120 min, the intracellular rate of viable bacteria was however under 15%, suggesting bacteria phagocytosis and degradation (**Figure SI-4-F**). Compared to the bacteria control, Cb-MSCs rate within the macrophage cytoplasm was higher (≈ 2.55-fold *versus* Cb; p<0.01), while no difference was observed between Ci-MSCs and Ci (**Figure 6B**). Taken together, these

results indicate that Cb-MSCs and Ci-MSCs are phagocyted by macrophages, but Cb-MSCs seem resistant to the macrophage degradation. It was suggested that low-grade and chronic *C. acnes* infections result in the persistence of bacteria inside immune cells.[3,7,52] Few studies have reported that *C. acnes* is capable of surviving intracellularly in professional phagocytes.[3,7,53] To confirm the resistance of Cb-MSCs to the macrophage degradation, infected THP-1 were maintained in culture for 24 h. The results revealed that the rate of viable Cb-MSCs in macrophage was still higher (≈ 2-fold *versus* Cb; $p<0.01$), while the rate of viable Ci-MSCs dropped significantly (≈ 0.32-fold *versus* Ci; $p<0.01$), signature of bacteria degradation (**Figure 6C**). Surprisingly, in comparison with Ci, the rate of Cb-MSCs in macrophage was higher (> 3-fold, $p<0.0001$). Taken together, our results confirm that commensal Cb following infection of MSCs acquires features that increase their resistance to degradation by macrophages.

Impact on the production of catalase by *C. acnes*:

Biochemical fingerprint of Cb-MSCs, suggesting the reduction in the glucan content could provide partial explanation on macrophage persistence of Cb-MSCs. It is well known that the production of reactive oxygen species (ROS) is a central mechanism used by phagocytes to kill bacteria. However, bacterial catalase, antioxidant enzyme, may cope with metabolic-derived ROS and thus increase the bacteria survival in cytoplasm.[54] To decipher the bacteria persistence in macrophage, the intracellular accumulation of ROS within infected macrophage and catalase production by Cb-MSCs and Ci-MSCs were evaluated. Compared to non-infected macrophage, no significant increase in the intracellular accumulation of ROS in infected macrophages was noticed whatever the bacteria (**Figure 7A**, **Figure SI-5A-C**). However, our results

revealed that in contrast to Ci-MSCs, Cb-MSCs significantly increased the production of catalase (2-fold versus Cb, $p<0.002$) (**Figure 7B** and **Figure SI-5D**). Thus, the persistence of Cb-MSCs in macrophage could be a result of the bacterial wall modification but also of the imbalanced between intracellular ROS accumulation in macrophages and catalase production.

Invasion of bacteria in non-phagocytic host cells appears to be a critical mechanism of microbial persistence in host tissues. It is well known that Gram-positive bacteria are able to sense and withstand the myriad of environmental stresses and to survive particularly within a host, establishing and maintaining infection. One key to their survival lies in their ability to respond efficiently to different and fast changing environments by shaping their envelop and transcriptome in response to environmental conditions.[55-57] Despite the ongoing controversies concerning the origin of *C. acnes* infections (*i.e.* leakage of bacteria from the superficial skin into the surgical wound *versus* the localization of *C. acnes* in the intracellular compartment of bone stromal cells), we demonstrated in this study that non-phagocytic bone marrow derived stromal cells could play a role in the propagation of *C. acnes* related osteomyelitis infection. Although the biochemical fingerprint of Cb-MSCs did not reveal the presence of stress markers, we thought MSCs cytoplasm had imposed an environmental stress to Cb. The resulting Cb-MSCs have therefore adapted through the modifications in the wall bacterial features and metabolic adaptation (*i.e.* an increase in the catalase production), reaching the features of pathogenic Ci. All these adaptive mechanisms resulted in the increase in the biofilm formation along with the increase in the invasion of osteoblast and persistence in macrophage. To decipher the relationship between bone marrow derived MSCs and *C. acnes* stressosome, a genomic and proteomic analyses should be performed.

Conclusion

In conclusion, this study provides insights on bone implant-associated infections through the interaction of clinical commensal *C. acnes* with bone marrow-derived mesenchymal stem cells. Commensal *C. acnes* were able to invade MSCs and to affect their paracrine activities, promoting the secretion of immunomodulatory mediators such as PGE2 and IDO. Therefore, *C. acnes* infected-bone marrow MSCs might establish a regenerative microenvironment to support bone healing and prosthesis integration instead of fighting the bacteria infection, suggesting that local treatment with autologous bone marrow-MSCs during bone reconstructive surgery could increase the risk of implant-related infection. Additionally, we demonstrated that *C. acnes*/ MSCs interaction induced a potential transition of commensal *C. acnes* to an opportunistic pathogen. Indeed, along with changes in the biochemical fingerprint, catalase production and wall nanofeatures of the intracellular *C. acnes*, herein we observed that intracellular *C. acnes* increased the biofilm formation on orthopaedical material (*i.e*. titanium alloy and PEEK), increased the invasiveness of osteoblasts and the resistance of macrophage degradation. Additional experiments, using a large panel of clinical strains with different multilocus sequence typing and phylotypes are required to state about the effect of bone marrow derived mesenchymal stem cells on the transition of commensal *C. acnes* to an opportunistic pathogen. Furthermore, in large scale future studies, the investigation of the potential strategies to block the *C. acnes*/MSCs interaction and internalization might decrease the risk of chronic osteomyelitis infections.

Acknowledgments

This work was supported by «Region Grand Est, Fonds Régional de Coopération pour la Recherche-ERMES». The authors are very grateful to the staff of service of traumatology (Dr. S. Diallo), Reims Hospital for providing human bone marrow samples, to the service of Bacteriology of Reims Hospital (Pr. C. De Champs, Dr. V. Vernet-Garnier) for providing *C. acnes* clinical strains and Mrs M. Cantener (English teacher from Odontology faculty of Reims) for their careful reading of the manuscript. The authors also thank the Spectroscopy and Microscopy of Interfaces Service Facility (SMI) of LCPME where the IR-ATR and AFM measurements were performed (Université de Lorraine-CNRS– http://www.lcpme.cnrs-nancy.fr; LCPME, UMR7564, 405 rue de Vandoeuvre 54600, France), E. Mathieu from INSERM U1121 (Université de Strasbourg, France) and L. Wortham from PICT Reims Champagne-Ardenne for technical help concerning transmission electron microscopy, Dr. F. Velard for scanning electron microscopy imaging and Dr. C. Terryn for confocal microscopy imaging (PICT Reims Champagne-Ardenne).

References

[1] C. Torrens, R. Marí, A. Alier, L. Puig, F. Santana, S. Corvec, Cutibacterium acnes in primary reverse shoulder arthroplasty: from skin to deep layers. J. Shoulder Elbow Surg. 28 (2019) 839–846.

[2] Y. Achermann, E. J. C. Goldstein, T. Coenye, M. E. Shirtliff, Propionibacterium acnes: from Commensal to Opportunistic Biofilm-Associated Implant Pathogen. Clin. Microbiol. Rev. 27 (2014) 419–440.

[3] C. Mayslich, P. A. Grange, N. Dupin, Cutibacterium acnes as an Opportunistic Pathogen: An Update of Its Virulence-Associated Factors. Microorganisms 9 (2021) 303.

[4] G. S. Hall, K. Pratt-Rippin, D. M. Meisler, J. A. Washington, T. J. Roussel, D.

Miller, Growth curve for Propionibacterium acnes. Curr. Eye Res. 13 (1994) 465–466.

[5] L. Pauzenberger, V. Heller, R. C. Ostermann, B. Laky, P. R. Heuberer, W. Anderl, Cutibacterium Acnes (Formerly Propionibacterium Acnes) Contamination of the Surgical Field During Shoulder Arthroscopy. Arthroscopy 35 (2019) 1750–1757.

[6] N. Heckmann, L. Sivasundaram, K. S. Heidari, A. E. Weber, E. N. Mayer, R. Omid, C. T. Vangsness, G. F. Hatch, Propionibacterium Acnes Persists Despite Various Skin Preparation Techniques. Arthroscopy 34 (2018) 1786–1789.

[7] R. Hudek, A. Brobeil, H. Brüggemann, F. Sommer, S. Gattenlöhner, F. Gohlke, Cutibacterium acnes is an intracellular and intra-articular commensal of the human shoulder joint. J. Shoulder Elbow Surg. 30 (2021) 16–26.

[8] R. Hudek, F. Sommer, M. Kerwat, A. F. Abdelkawi, F. Loos, F. Gohlke, Propionibacterium acnes in shoulder surgery: true infection, contamination, or commensal of the deep tissue? J. Shoulder Elbow Surg. 23 (2014) 1763–1771.

[9] S. Brandau, M. Jakob, K. Bruderek, F. Bootz, B. Giebel, S. Radtke, K. Mauel, M. Jäger, S. B. Flohé, S. Lang, Mesenchymal Stem Cells Augment the Anti-Bacterial Activity of Neutrophil Granulocytes. PLOS ONE 9 (2014) e106903.

[10] R. Ramezankhani, R. Solhi, A. Memarnejadian, F. Nami, S. M. R. Hashemian, T. Tricot, M. Vosough, C. Verfaillie, Therapeutic modalities and novel approaches in regenerative medicine for COVID-19. Int. J. Antimicrob. Agents 56 (2020) 106208.

[11] Y. Wang, X. Chen, W. Cao, Y. Shi, Plasticity of mesenchymal stem cells in immunomodulation: pathological and therapeutic implications. Nat. Immunol. 15 (2014) 1009–1016.

[12] A. I. Caplan, D. Correa, The MSC: an injury drugstore. Cell Stem Cell 9 (2011) 11–15.

[13] E. Seebach, J. Holschbach, N. Buchta, R.G. Bitsch, K. Kleinschmidt, W. Richter, Mesenchymal stromal cell implantation for stimulation of long bone healing aggravates Staphylococcus aureus induced osteomyelitis. Acta Biomater. 21, (2015) 165–177.

[14] J. Yoshitani, T. Kabata, H. Arakawa, Y. Kato, T. Nojima, K. Hayashi, M. Tokoro, N. Sugimoto, Y. Kajino, D. Inoue, *et al.* Combinational therapy with antibiotics and antibiotic-loaded adipose-derived stem cells reduce abscess formation in implant-related infection in rats. *Sci. Rep.* 10 (2020) 11182.

[15] M. Dubus, J. Varin, S. Papa, H. Rammal, J. Chevrier, E. Maisonneuve, C. Mauprivez, C. Mongaret, S. C. Gangloff, F. Reffuveille, *et al.* Interaction of Cutibacterium acnes with human bone marrow derived mesenchymal stem cells: a step toward understanding bone implant- associated infection development. Acta Biomater. 104 (2020) 124–134.

[16] M. Dubus, J. Varin-Simon, P. Prada, L. Scomazzon, F. Reffuveille, H. Alem, F.

Boulmedais, C. Mauprivez, H. Rammal, H. Kerdjoudj, Biopolymers-calcium phosphate antibacterial coating reduces the pathogenicity of internalized bacteria by mesenchymal stromal cells. Biomater. Sci. 8 (2020) 5763–5773.

[17] T. S. El-Mahdy, C. Mongaret, J. Varin-Simon, F. Lamret, V. Vernet-Garnier, H. Rammal, C. Mauprivez, H. Kerdjoudj, S. C. Gangloff, F. Reffuveille, Interaction of implant infection-related commensal bacteria with mesenchymal stem cells: a comparison between Cutibacterium acnes and Staphylococcus aureus. FEMS Microbiol. Lett. 368 (2021) fnab014.

[18] G. G. Aubin, M. Baud'huin, J. P. Lavigne, R. Brion, F. Gouin, D. Lepelletier, C. Jacqueline, D. Heymann, K. Asehnoune, S. Corvec, Interaction of Cutibacterium (formerly Propionibacterium) acnes with bone cells: a step toward understanding bone and joint infection development. Sci. Rep. 7, (2017) 42918.

[19] I. N. Sneddon, The relation between load and penetration in the axisymmetric boussinesq problem for a punch of arbitrary profile. Int. J. Eng. Sci. 3 (1965) 47–57.

[20] N. Gavara, R. S. Chadwick, Determination of the elastic moduli of thin samples and adherent cells using conical atomic force microscope tips. Nat. Nanotechnol. 7 (2012) 733–736.

[21] P. Polyakov, C. Soussen, J. Duan, J. F. L. Duval, D. Brie, G. Francius, Automated Force Volume Image Processing for Biological Samples. PLoS ONE 6 (2011) e18887.

[22] G. G. Aubin, J. P. Lavigne, Y. Foucher, S. Dellière, D. Lepelletier, F. Gouin, S. Corvec, Tropism and virulence of Cutibacterium (formerly Propionibacterium) acnes involved in implant-associated infection. Anaerobe 47 (2017) 73–78.

[23] R. Bayston, B. Nuradeen, W. Ashraf, B. J. C. Freeman, Antibiotics for the eradication of Propionibacterium acnes biofilms in surgical infection. J. Antimicrob. Chemother. 60 (2007) 1298–1301.

[24] A. Holmberg, R. Lood, M. Mörgelin, B. Söderquist, E. Holst, M. Collin, B. Christensson, M. A. Rasmussen, Biofilm formation by Propionibacterium acnes is a characteristic of invasive isolates. Clin. Microbiol. Infect. 15 (2009) 787–795.

[25] E. Platsidaki, C. Dessinioti, Recent advances in understanding Propionibacterium acnes (Cutibacterium acnes) in acne. F1000Research 7 (2018) F1000.

[26] E. Maisonneuve, J. Chevrier, M. Dubus, J. Varin, J. Sergheraert, S. C. Gangloff, F. Reffuveille, C. Mauprivez, H. Kerdjoudj, Infection of Human Dental Pulp Stromal Cells by Streptococcus mutans: Shedding Light on Bacteria Pathogenicity and Pulp Inflammation. Front. Cell Dev. Biol. 8 (2020) 785.

[27] J. Josse, F. Velard, S. Mechiche Alami, V. Brun, C. Guillaume, H. Kerdjoudj, B, Lamkhioued, S. C. Gangloff, Increased internalization of Staphylococcus aureus and cytokine expression in human Wharton's jelly mesenchymal stem cells. Biomed. Mater. Eng. 24 (2014) 27–35.

[28] N. Alva-Murillo, J. E. López-Meza, A. Ochoa-Zarzosa, Nonprofessional Phagocytic Cell Receptors Involved in Staphylococcus aureus Internalization. BioMed Res. Int. 2014 (2014) 538546.

[29] J. Gruenberg, F. G. van der Goot, Mechanisms of pathogen entry through the endosomal compartments. Nat. Rev. Mol. Cell Biol. 7 (2006) 495–504.

[30] J. M. Berthelot, S. Corvec, G. Hayem, SAPHO, autophagy, IL-1, FoxO1, and Propionibacterium (Cutibacterium) acnes. Joint Bone Spine 85 (2018) 171–176.

[31] M. Rajagopal, S. Walker, Envelope Structures of Gram-Positive Bacteria. Curr. Top. Microbiol. Immunol. 404 (2017) 1–44.

[32] A. J. Wolf, D. M. Underhill, Peptidoglycan recognition by the innate immune system. Nat. Rev. Immunol. 18 (2018) 243–254.

[33] S. Brown, J. P. Santa Maria, S. Walker, Wall Teichoic Acids of Gram-Positive Bacteria. Annu. Rev. Microbiol. 67 (2013) 313-336.

[34] D. Naumann, Ft-Infrared and Ft-Raman Spectroscopy in Biomedical Research. Appl. Spectrosc. Rev. 36 (2001) 239–298.

[35] F. Quilès, D. Barth, O. Peric, G. E. Fantner, G. Francius, Parietal Structures of Escherichia coli Can Impact the D-Cateslytin Antibacterial Activity. ACS Chem. Biol. 15 (2020) 2801–2814.

[36] S. Wongthong, P. Tippayawat, M. Wongwattanakul, P. Poung-ngern, L. Wonglakorn, A. Chanawong, P. Heraud, A. Lulitanond, Attenuated total reflection: Fourier transform infrared spectroscopy for detection of heterogeneous vancomycin—intermediate Staphylococcus aureus. World J. Microbiol. Biotechnol. 36 (2020) 22.

[37] E. Yunda, F. Quilès, In situ spectroscopic analysis of Lactobacillus rhamnosus GG flow on an abiotic surface reveals a role for nutrients in biofilm development. Biofouling 35 (2019) 494–507.

[38] K. Bahmed, F. Quilès, R. Bonaly, J. Coulon, Fluorescence and infrared spectrometric study of cell walls from Candida, kluyveromyces, Rhodotorula and schizosaccharomyces yeasts in relation with their chemical composition. Biomacromolecules 4 (2003) 1763–1772.

[39] J. H. Hong, H. K. Jung, Antioxidant and antitumor activities of β-glucan-rich exopolysaccharides with different molecular weight from Paenibacillus polymyxa JB115. J. Korean Soc. Appl. Biol. Chem. 57 (2014) 105–112.

[40] L. Xu, J. Zhang, Bacterial glucans: production, properties, and applications. Appl. Microbiol. Biotechnol. 100 (2016) 9023–9036.

[41] P. Rusek, M. Wala, M. Druszczyńska, M. Fol, Infectious Agents as Stimuli of Trained Innate Immunity. Int. J. Mol. Sci. 19 (2018) 456.

[42] M. T. Sutton, D. Fletcher, S. K. Ghosh, A. Weinberg, R. van Heeckeren, S. Kaur, Z. Sadeghi, A. Hijaz, J. Reese, H. M. Lazarus, *et al.* Antimicrobial Properties of Mesenchymal Stem Cells: Therapeutic Potential for Cystic Fibrosis Infection, and Treatment. Stem Cell International. 2016 (2016) 12.

[43] É. Mezey, K. Nemeth, Mesenchymal stem cells and infectious diseases: Smarter than drugs. Immunol. Lett. 168 (2015) 208–214.

[44] G. Jarute, A. Kainz, G. Schroll, J. R. Baena, B. Lendl, On-line determination of the intracellular poly(beta-hydroxybutyric acid) content in transformed Escherichia coli and glucose during PHB production using stopped-flow attenuated total reflection FT-IR spectrometry. Anal. Chem. 76 (2004) 6353–6358.

[45] F. Quilès, F. Humbert, On the production of glycogen by Pseudomonas fluorescens during biofilm development: an in situ study by attenuated total reflection-infrared with chemometrics. Biofouling 30 (2014) 709–718.

[46] C. T. Kreis, R. M. A. Sullan, Interfacial nanomechanical heterogeneity of the E. coli biofilm matrix. Nanoscale 12 (2020) 16819–16830.

[47] S. C. Uzoechi, N. I. Abu-Lail, Changes in cellular elasticities and conformational properties of bacterial surface biopolymers of multidrug-resistant Escherichia coli (MDR-E. coli) strains in response to ampicillin. Cell Surf. 5 (2019) 100019.

[48] F. Quilès, P. Polyakov, F. Humbert, G. Francius, Production of Extracellular Glycogen by Pseudomonas fluorescens: Spectroscopic Evidence and Conformational Analysis by Biomolecular Recognition. Biomacromolecules 13 (2012) 2118–2127.

[49] G. Francius, S. Lebeer, D. Alsteens, L. Wildling, H. J. Gruber, P. Hols, S. De Keersmaecker, J. Vanderleyden, Y. F. Dufrêne, Detection, localization, and conformational analysis of single polysaccharide molecules on live bacteria. ACS Nano 2 (2008) 1921–1929.

[50] G. Ramage, M. M. Tunney, S. Patrick, S. P. Gorman, J. R. Nixon, Formation of Propionibacterium acnes biofilms on orthopaedic biomaterials and their susceptibility to antimicrobials. Biomaterials 24 (2003) 3221–3227.

[51] T. Coenye, E. Peeters, H. J. Nelis, Biofilm formation by Propionibacterium acnes is associated with increased resistance to antimicrobial agents and increased production of putative virulence factors. Res. Microbiol. 158 (2007) 386–392.

[52] E. Contassot, L. E. French, New Insights into Acne Pathogenesis: Propionibacterium Acnes Activates the Inflammasome. J. Invest. Dermatol. 134 (2014) 310–313.

[53] Y. Bae, T. Ito, T. Iida, K. Uchida, M. Sekine, Y. Nakajima, J. Kumagai, T. Yokoyama, H. Kawachi, T. Akashi, *et al.* Intracellular Propionibacterium acnes Infection in Glandular Epithelium and Stromal Macrophages of the Prostate with or without Cancer. PLOS ONE 9 (2014) e90324.

[54] K. Yamamoto, K. Uchida, A. Furukawa, T. Tamura, Y. Ishige, M. Negi, D. Kobayashi, T. Ito, T. Kakegawa, A. Hebisawa, et al. Catalase expression of Propionibacterium acnes may contribute to intracellular persistence of the bacterium in sinus macrophages of lymph nodes affected by sarcoidosis. Immunol. Res. 67 (2019) 182–193.

[55] C. Guldimann, K. J. Boor, M. Wiedmann, V. Guariglia-Oropeza, Resilience in the Face of Uncertainty: Sigma Factor B Fine-Tunes Gene Expression To Support Homeostasis in Gram-Positive Bacteria. Appl. Environ. Microbiol. 82 (2016) 4456–4469.

[56] C. Y. Bonilla, Generally Stressed Out Bacteria: Environmental Stress Response Mechanisms in Gram-Positive Bacteria. Integr. Comp. Biol. 60 (2020) 126–133.

[57] C. L. Hews, T. Cho, G. Rowley, T. L. Raivio, Maintaining Integrity Under Stress: Envelope Stress Response Regulation of Pathogenesis in Gram-Negative Bacteria. Front. Cell. Infect. Microbiol. 9 (2019) 313.

Figure captions

Figure 1: *C. acnes*/ MSCs interaction. (A) Percentage of the viable intracellular bacteria after 3 h of contact with MSCs, indicating a higher invasiveness of Ci *versus* Cb ($, Ci *vs* Cb, p=0.01). (B) Transmission electron microscopy picture of MSCs infected with *C. acnes,* showing the intracellular bacteria (black square; scale bars = 600 and 500 nm). (C) Confocal laser scanning microscopy and orthogonal view of cytoskeleton of MSCs infected with *C. acnes* with Phalloidin-coupled to Alexa® 488 (green color) and DNA labelled with DAPI (magenta color). White arrows indicate bacterial DNA. (D) Scanning electron microscopy picture of MSCs infected with *C. acnes,* showing adhered bacteria to the MSCs membrane (black square, scale bars = 10 and 1 μm). (E) Percentage of the viable intracellular bacteria after 3 h of contact with cytochalasin-D treated MSCs, indicating a lower invasiveness capability *versus* MSCs control (*i.e.* MSCs non treated with cyto-D) (Histograms of mean ± SEM, n = 6, Mann & Whitney test).

Figure 2: Immunomodulatory profile of *C. acnes* infected MSCs. ELISA quantification assay of released Prostaglandin E-2 (A) and Indolamine 2,3 dioxygenase (B), showing an increase in an anti-inflammatory profile of Cb-infected MSCs. (Histograms of mean ± SEM, n = 6, Mann & Whitney test; (*), infected MSCs *versus* MSCs control, $p < 0.01$).

Figure 3: Infrared spectra in Attenuated Total Reflectance mode of *C. acnes* maintained in phosphate buffer solution. Black spectra highlight bacteria control while the grey spectra indicate intracellular bacteria. Upper box corresponds to Cb and Cb-MSCs strains and bottom box corresponds to Ci and Ci-MSCs strains. Main assignments are indicated. ν: stretching; δ: bending; a antisymmetric; s: symmetric. Spectra are normalized to the amide II band allowing the comparison of spectra.

Figure 4: Nanoscale characterization. (A) Atomic force microscopy imaging of *C. acnes* following MSCs infection (scale bars = 3 μm). (B-D) Contour length, adhesive forces and bacterial elasticity of the bacteria wall, revealing deep changes in Cb-infected MSCs features. (Histograms of mean ± SEM, n = 3, Mann & Whitney test; (*), bacteria following MSCs infection *versus* bacteria control, $p < 0.0001$).

Figure 5: Biofilm formation. (A) Crystal violet assay on Titanium alloy (TA6V), 316L stainless steel (316L SS), polyetheretherketone (PEEK) and Type I collagen, showing that the bacteria behavior is strongly linked to the biomaterial. Data normalized to bacteria control (non-exposed *C. acnes* to MSCs; red dashed line; Histograms of mean ± SEM, n = 6, Mann & Whitney test; ($), Ci *versus* Cb, p=0.01). (B) Representative images of biofilms obtained by confocal laser scanning microscopy. Alive bacteria in green and damaged bacteria in red. (scale bars = 50 μm).

Figure 6: *C. acnes*/bone cells interactions. (A) Viable intracellular bacteria after 3 h of contact with osteoblasts, indicating a higher invasiveness of Cb-MSCs *versus* Ci-MSCs. (B) Viable intracellular

bacteria after 2 h of contact with differentiated THP-1 and (C) Viable intracellular bacteria after 24 h of contact with differentiated THP-1, revealing the persistence of Cb-MSCs in macrophage cytoplasm. Data normalized to bacteria control (non-exposed *C. acnes* to MSCs highlighted by the red dashed lines; Histograms of mean ± SEM, n = 4, Mann & Whitney test; (£), Cb *versus* Cb-MSCs, p=0.01).

Figure 7: Reactive oxygen species accumulation and catalase activity. (A) Intracellular accumulation of ROS in infected macrophages. (B) Catalase activity of viable intracellular *C. acnes*, showing an imbalance between intracellular ROS accumulation Cb-MSCs-macrophage and Cb-MSCs catalase production. Data normalized to bacteria control (non-exposed *C. acnes* to MSCs highlighted by the red dashed lines; Histograms of mean ± SEM, n = 4, Mann & Whitney test; ($), Cb-MSCs *versus* Cb, p<0.002).

Figure 1

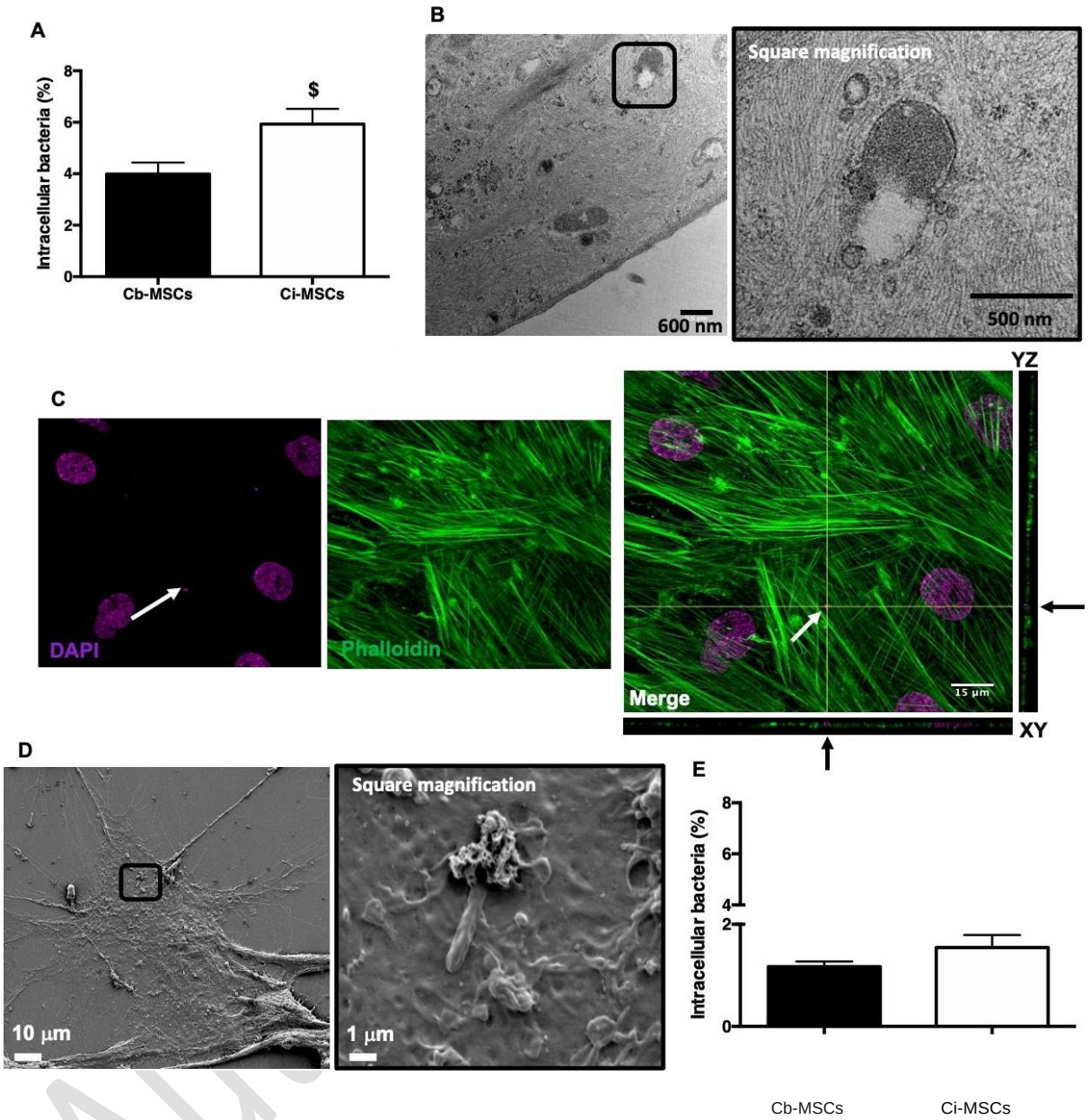
A
Intracellular bacteria (%)
8
6
4
2
0
$
Cb-MSCs
Ci-MSCs
B
600 nm
Square magnification
500 nm
C
DAPI
Phalloidin
Merge
15 µm
YZ
XY
D
10 µm
Square magnification
1 µm
E
Intracellular bacteria (%)
8
6
4
2
0
Cb-MSCs
Ci-MSCs

Figure 2

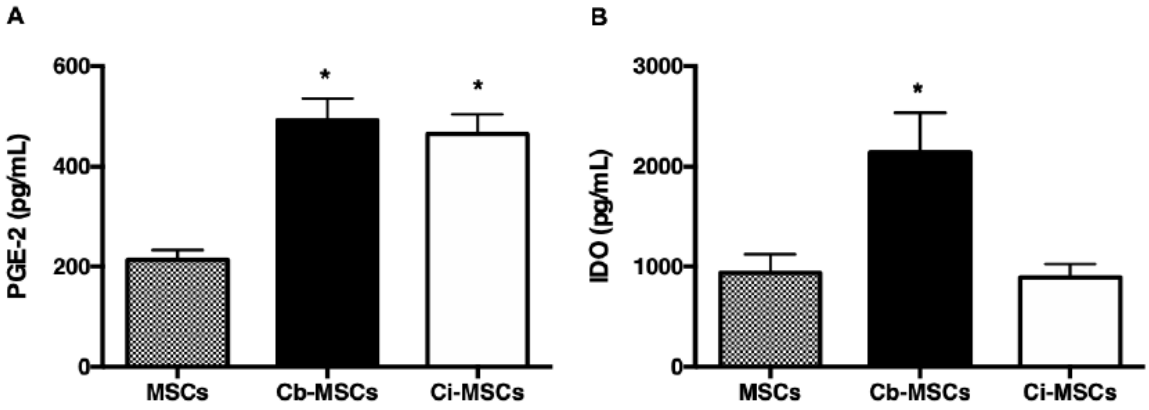

Figure 3

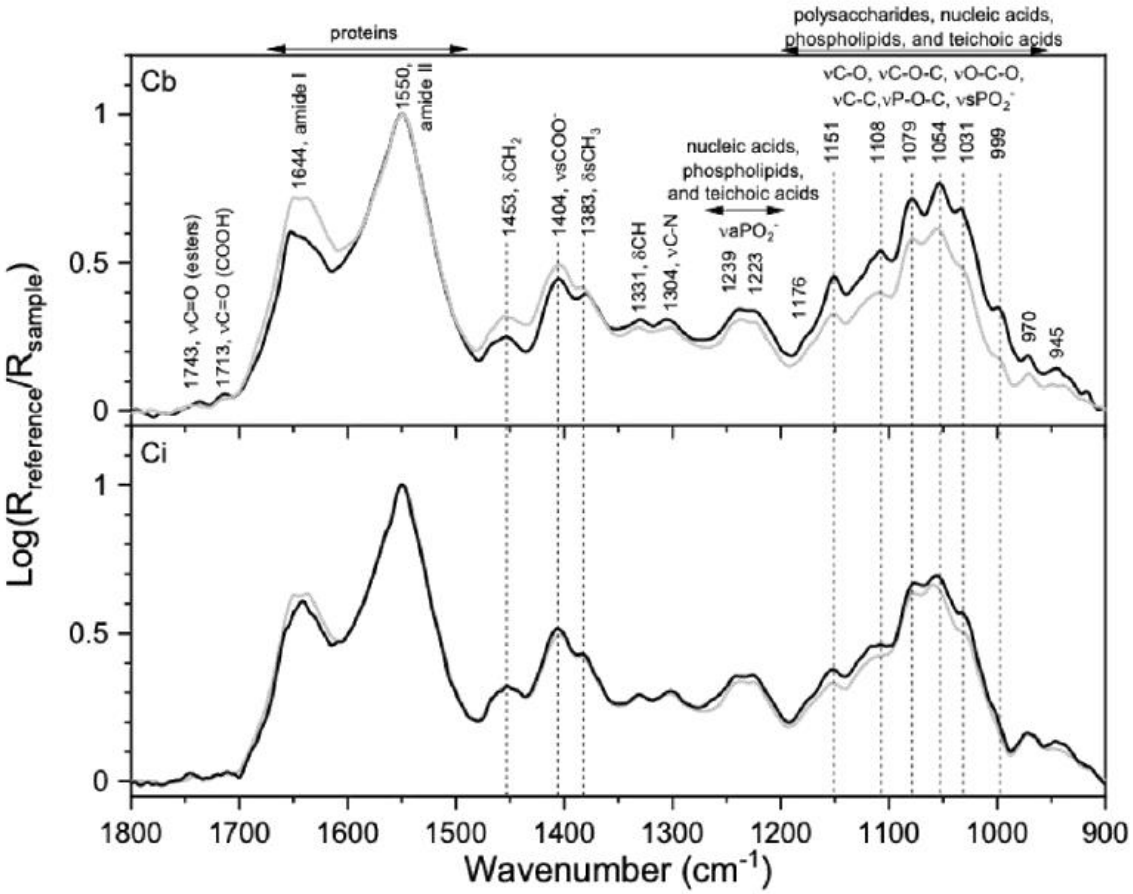
proteins
polysaccharides, nucleic acids, phospholipids, and teichoic acids
Cb
Ci
1743, νC=O (esters)
1713, νC=O (COOH)
1644, amide I
1550, amide II
1453, δCH2
1404, νsCOO-
1383, δsCH3
1331, δCH
1304, νC-N
nucleic acids, phospholipids, and teichoic acids
νaPO2-
1239
1223
1176
νC-O, νC-O-C, νO-C-O, νC-C, νP-O-C, νsPO2-
1151
1108
1079
1054
1031
999
970
945
Log(Rreference/Rsample)
Wavenumber (cm-1)

Figure 4

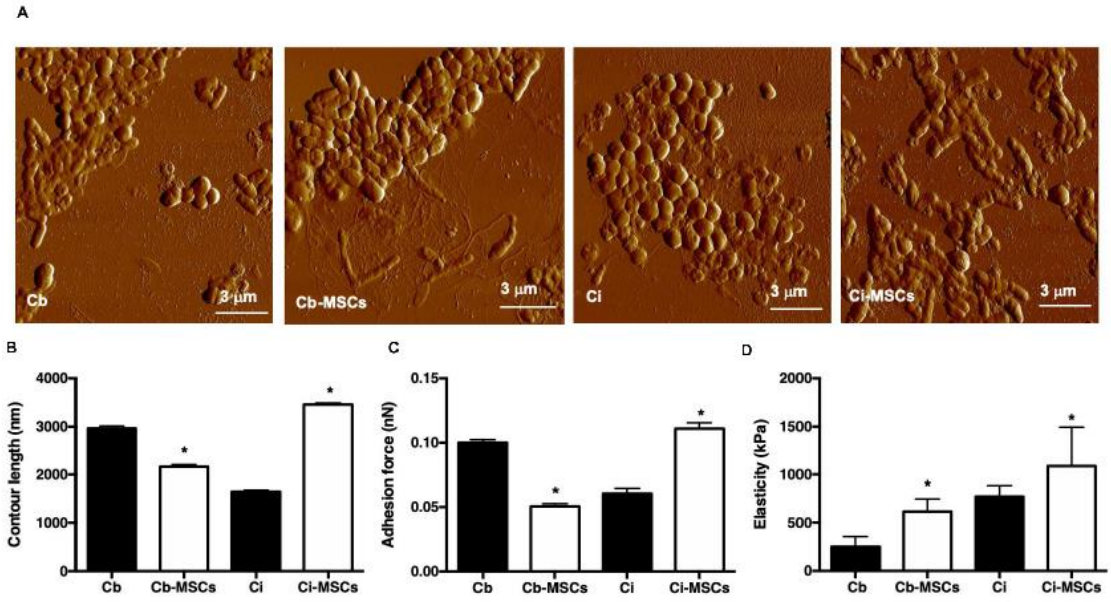

Figure 5

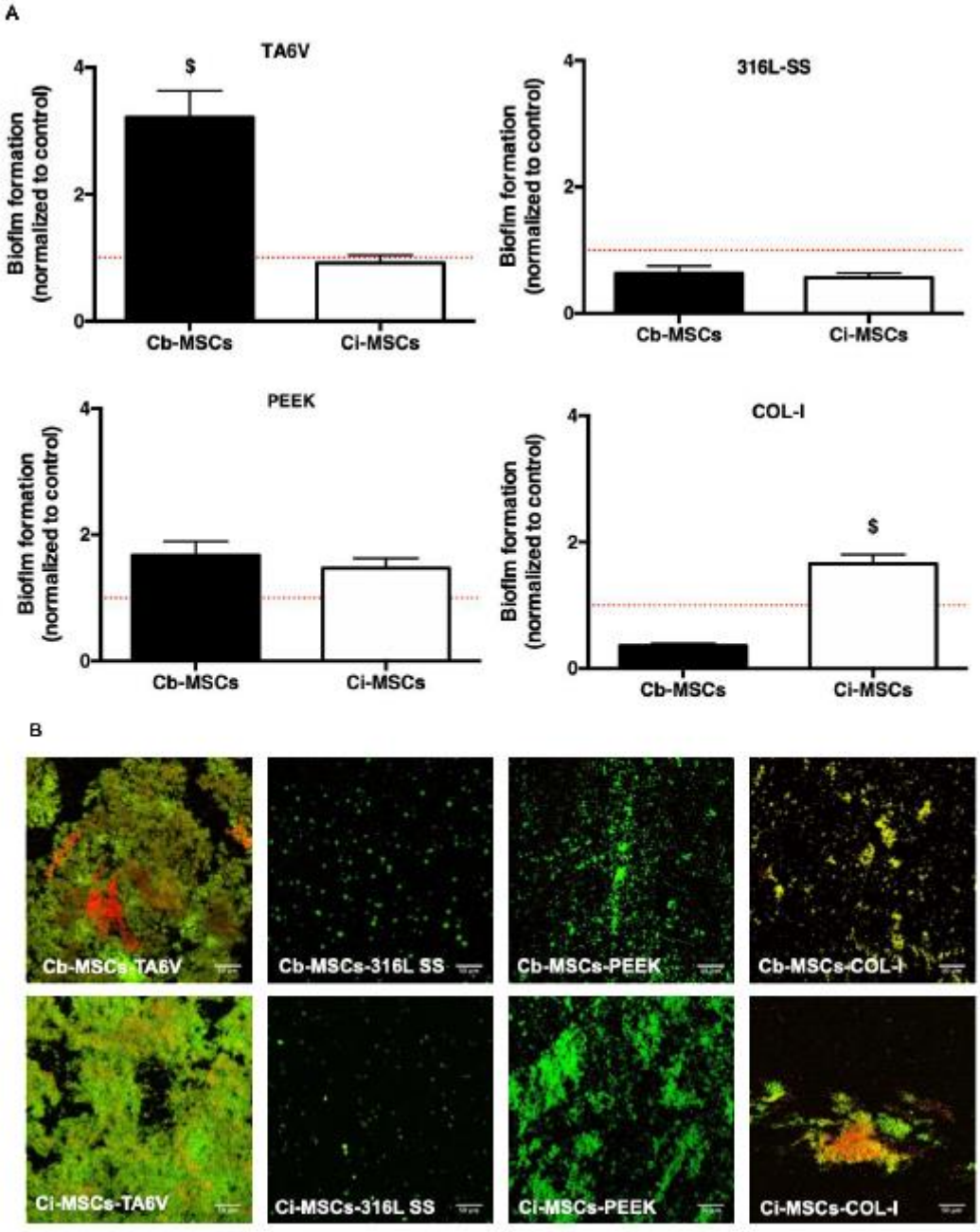
A
TA6V
316L-SS
PEEK
COL-I
Biofilm formation (normalized to control)
$
Cb-MSCs
Ci-MSCs
B
Cb-MSCs-TA6V
Cb-MSCs-316L SS
Cb-MSCs-PEEK
Cb-MSCs-COL-I
Ci-MSCs-TA6V
Ci-MSCs-316L SS
Ci-MSCs-PEEK
Ci-MSCs-COL-I

Figure 6

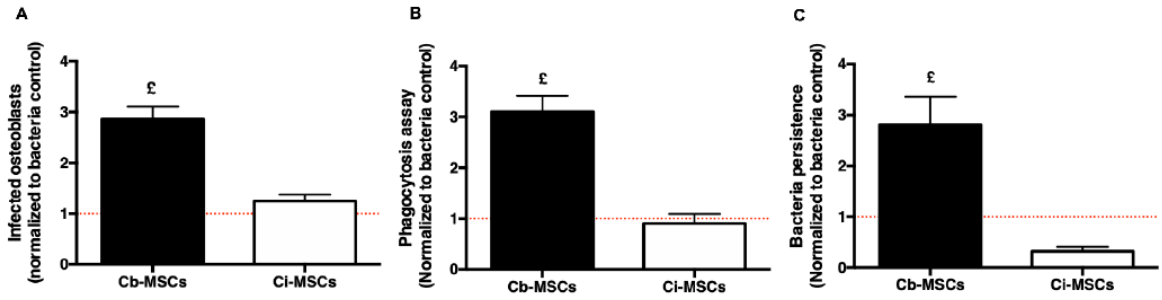

Figure 7